JOURNAL OF MATERIALS SCIENCE 22 (1987) 803–817

The development of dislocation substructure in hydrogen embrittled niobium–8 to 10 at% vanadium alloy

Part 1

K. JAGANNADHAM
Materials Science and Engineering Department, North Carolina State University, Raleigh, North Carolina 27695, USA

FRANCIS C. LAABS
Metallurgy and Ceramics Division, Ames Laboratory, Ames, Iowa 50011, USA

The development of dislocation substructure in niobium–8 to 10 at% vanadium alloy single and polycrystals is presented to emphasize the effect of interstitial hydrogen and substitutional vanadium. The formation of cross grid of straight long screw dislocations in the initial stages of deformation is associated with a high lattice frictional stress caused by the substitutional vanadium. Similarly, the presence of non-screw segments, edge dipoles and loop debris at higher strains is also considered to arise from the high lattice frictional stress. On the other hand, the formation of cell structure at 195 K in both single and polycrystals tested in tension is related to the presence of hydrogen. In addition, the nucleation of cracks along the active {1 0 1} or {1 1 2} type slip planes is related to the accumulation of hydrogen atoms along cell walls. Furthermore, the stress concentration due to the array of long straight dislocations is believed responsible for twinning observed at 77 K in the presence of hydrogen. The dislocation substructure associated with deformation twins indicates that hydrogen embrittlement through crack nucleation cannot be linked with deformation twinning in this alloy.

1. Introduction

In order to gain a better understanding of the mechanisms of embrittlement due to interstitial solute hydrogen atoms, recent research efforts have resorted to a more direct observation of *in situ* deformed foils in the transmission electron microscope equipped with a special environment cell [1, 2]. A unique feature of these observations that seems to emerge very strongly is that they further support the idea that hydrogen in solid solution causes enhanced localized plastic deformation [3] through the increased mobility of screw dislocations at room temperature. Whereas certain quantitative determinations of dislocation density in macroscopic samples [4, 5] seem to confirm this view, a few other observations illustrate that the scale of dislocation substructural features as well as the density are not very much effected [6, 7]. The foils observed *in situ* in the transmission electron microscope are relatively thin (less than 1 μm) compared to the macroscopic specimens [2, 8] and thus plane stress conditions exist during tensile deformation. The effects produced by the free surface in adsorbing interstitials and in exerting image forces that influence dislocation multiplication and mobility are not completely clear. A significant difference in the behaviour of cracks has been noticed in foils of different thickness deformed *in situ* in a high voltage microscope [9]. In addition, all observations of enhanced dislocation mobility in the *in situ* deformed foils are reported in iron which has low hydrogen solid solubility [10].

On the other hand, refractory alloys of niobium and vanadium possess a larger interstitial solid solubility of hydrogen [11]. This paper presents electron microscopic observations in the niobium–8 to 10 at% vanadium alloy to determine the effect of high hydrogen solubility on the development of dislocation substructure. Indeed, the observations of dislocation substructure in tantalum containing nitrogen [12] and deformed in tension at 77 K have lead to the conclusion that the interaction of the stress field of the dislocation with the tetragonal distortion associated with the interstitial atom increases the frictional stress to movement at both edge and screw type dislocations equally. However, the decreasing incidence of cross slip of screw dislocations is a more important effect that lead to a dislocation substructure consisting mainly of long straight screw dislocations with very little loop debris. A theoretical estimation of enhancement of concentration of hydrogen atoms around a dislocation, due to its long-range stress field interaction, not including the core region shows a negligible contribution for a low dislocation density (small strain) but important effect at larger values (larger strains). This result implies large enhancement at lower temperatures provided hydrogen atoms can diffuse to the dislocation or to the crack tip [10, 13].

0022–2461/87 $03.00 + .12

It is well established that the core of a screw dislocation in bcc metals is dissociated on three {1 1 0} planes or two {1 1 2} planes belonging to a ⟨1 1 1⟩ zone and that recombination is required before dislocation movement [14]. This result is used to explain several features of low-temperature deformation such as slip geometry and orientation dependence of yield stress [15, 16]. The stacking fault energy, which enters into equilibrium equations of the dissociated configuration [15] is a function of the alloying element and composition. Hitherto, only three layered faults and twins have been observed [16] at the most in bcc metals indicating the presence of dissociation but at the same time the width of the dissociated configuration is not large enough to be resolved in the transmission electron microscope. However, there is mounting evidence to show that twinning becomes the mode of deformation at sufficiently low temperature (77 K) and with high concentration of interstitial hydrogen [17], an effect also observed in the presence of nitrogen in tantalum [12]. It has been found that twinning is absent in the niobium-rich vanadium alloy in the absence of a sufficiently large concentration of hydrogen but becomes a common observable feature in its presence and during deformation at low temperature (77 K) [17, 18]. Therefore, the present observations are used to determine whether interstitial hydrogen is effective in interacting with the dissociated configuration and thus in creating faulted regions and microtwins which are described as a stressed configuration of the core of the $0.5a$ ⟨1 1 1⟩ screw dislocation [19]. On the other hand, the stress concentration produced by an array of straight long screw dislocations is considered to be large enough to reduce the activation energy for nucleation and growth of a stable twin, particularly when slip is inhibited due to increased lattice friction stress in the presence of interstitial atoms [20, 21]. It is thought also useful to examine the dislocation substructure associated with the twinned configuration and thus to determine whether twins are nucleation centres for cracks [22].

Whereas the low-temperature brittle behaviour of pure bcc metals arises due to (0 0 1) cleavage, it has been found that hydrogen embrittlement of the niobium-rich vanadium alloy single crystals becomes severe at 195 K as a result of nucleation and growth of cracks along {1 1 0} or {1 1 2} operating slip planes in addition to the {0 0 1} type cleavage [17]. It is the aim of the present electron microscopic observations to determine if a close correspondence exists between the dislocation substructure in the presence of hydrogen and the observed crack planes.

2. Experimental procedure

Several single crystal and large grain size polycrystalline specimens were prepared by slicing from the bulk of this alloy obtained from electron beam melted purity of niobium and 5.74 wt % (10 at %) vanadium. Whereas the details of making the specimens, the method of charging with hydrogen and subsequent testing in tension are described elsewhere [21], it suffices to mention that the foils for transmission electron microscopic observations are made from the following.

(a) Single crystal C_2 with 150 p.p.m. hydrogen, 100 p.p.m. oxygen and 40 p.p.m. nitrogen, all in weight % and deformed in tension at 195 K.

(b) Single crystal 15_2 with no hydrogen, deformed in tension at 195 K.

(c) Polycrystalline specimens annealed at 1300° C for 3 h and deformed in tension at three different temperatures, 295, 195 and 77 K, and samples deformed in compression at 77 K.

Specifically, in order to determine the influence of increasing amounts of hydrogen, specimens charged with 200 p.p.m. and 400 p.p.m. wt % hydrogen deformed in tension either lightly, just above the yield point or up to necking and fracture are also examined. On the other hand, the compression specimens, 2 mm thick, were charged with 200 p.p.m. wt % hydrogen and deformed just above the yield point.

Single crystal specimens of 500 to 750 μm thickness were sliced parallel to either the primary or the secondary slip planes and were further spark cut into 3 mm diameter discs for preparation of the foils. Similarly, specimens in the form of 3 mm diameter discs were spark cut from polycrystalline specimens deformed either in tension or in compression and were further reduced to 500 to 750 μm thickness by means of grinding over a wheel covered with 320 grit silicon carbide paper. Further reduction in thickness to 300 μm was done by additional grinding over 600 grit silicon carbide paper. The specimens were subsequently electropolished in 6 vol % sulphuric acid in methanol to obtain 120 μm thickness foil with smooth and bright surfaces. Final thinning to produce perforation and electron transparent foil was made by jet thinning the discs using 6 vol % sulphuric acid in methanol containing 1 vol % hydrofluoric acid at an applied voltage of 100 V, 1 mm diameter jet and a temperature of $-50°$ C. The foil thickness varied near the very edge of the perforation but remained more uniform in the rest of the thinned area. A certain amount of loss of dislocations was observed in the areas of the foil close to the perforation and thus it was assumed to arise from smaller thickness. Observations of well-annealed foils did not show any introduction of dislocations during foil preparation, a result also substantiated from the dislocation substructures obtained and shown in Part 2. The foils obtained from single crystal specimens were examined in a side-entry double-tilt stage which is capable of tilting $\pm 55°$ about both the x- and y-axes in the plane of the foil but is eucentric with respect to only one tilt. The foils obtained from the polycrystalline samples were examined in a single tilt stage, again capable of tilting $\pm 55°$ about the x-axis parallel to the side entry. All the specimens were examined at 120 kV operating voltage in Jeol 100 CX transmission electron microscope.

3. Dislocation substructure in single crystals

3.1. Dislocation substructure in crystal C_2

The initial orientation of the tensile axis of the crystal is shown in Fig. 1 along with the poles of the observed

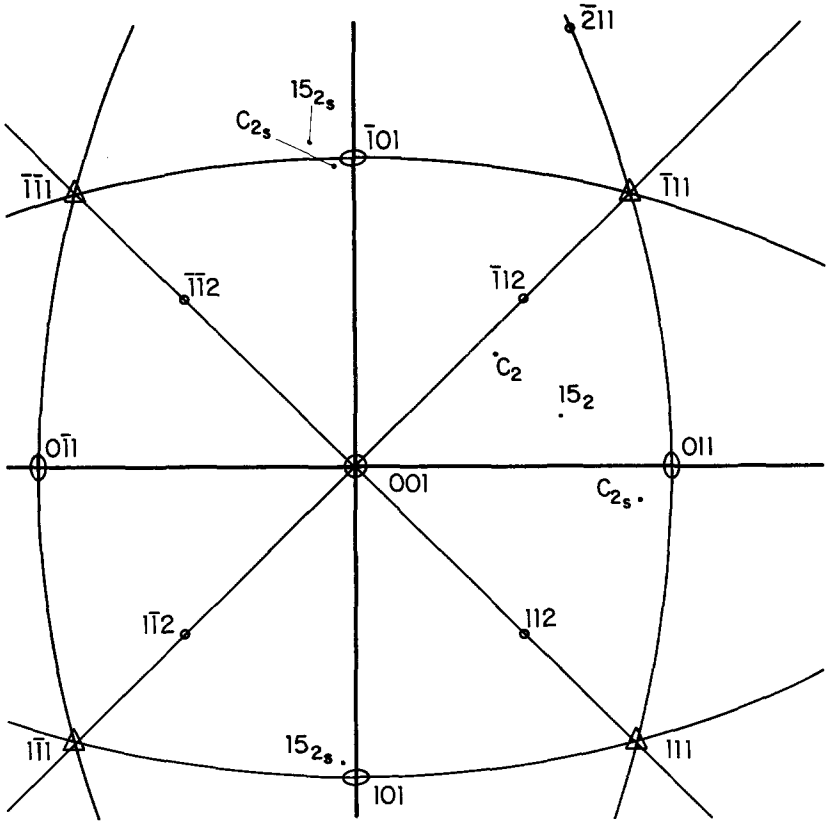

Figure 1 The (0 0 1) stereographic projection showing the orientation of the crystal C_2 charged with hydrogen and the crystal 15_2 of niobium–10 at % vanadium alloy. The observed slip systems are shown with subscript s.

primary ($\bar{1}$ 0 1) and the secondary (0 1 1) slip planes. Whereas a detailed description of the geometry of crystallographic nature of deformation of several single crystals is presented elsewhere [21], it is useful to point out that anomalous slip on the (0 $\bar{1}$ 1) plane has not been observed in all the crystals tested at 195 and 295 K. The identification of the Burgers vectors of the $0.5a\langle 1\,1\,1\rangle$ dislocations is carried out by examining the foil under various 1 0 1 and 1 1 2 type $\boldsymbol{g}$ vectors of the 1 0 1 and 1 1 1 type zone axis although such analysis is confined to only a few areas of the foil. Further, it is assumed that only $0.5a\langle 1\,1\,1\rangle$ type Burgers

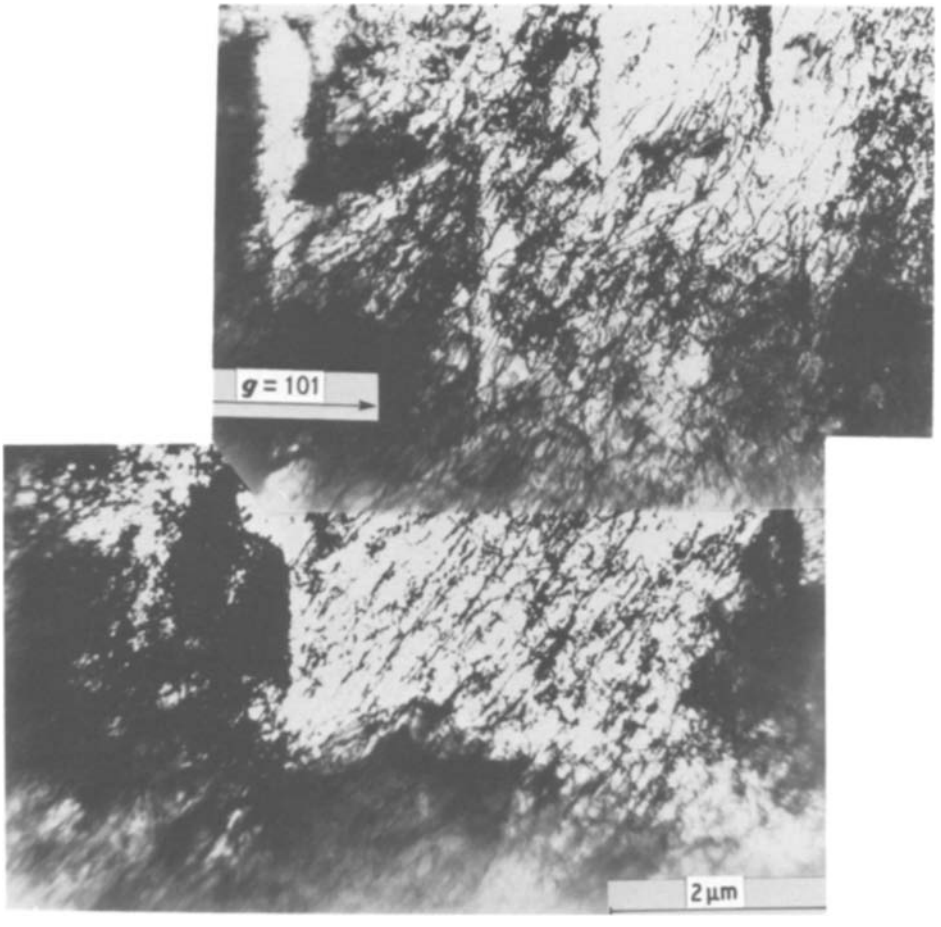

Figure 2 A low magnification electron micrograph of dislocation substructure observed in a foil cut parallel to a ($\bar{1}$ 0 1) plane in crystal C_2 of niobium–10 at % vanadium alloy with hydrogen. The foil contains predominantly dislocations of Burgers vector 1 1 1 and 1 $\bar{1}$ 1, $\boldsymbol{b} = \bar{8}17$.

vectors of dislocations are predominant with $a\langle 1\,0\,0\rangle$ type Burgers vectors of dislocations being formed as a result of suitable combination of $0.5a\langle 1\,1\,1\rangle$ type Burgers vectors of dislocations.

3.1.1. Foils parallel to $(\bar{1}\,0\,1)$ sections

A low magnification electron micrograph of the dislocation substructure of the foil is presented in Fig. 2 to illustrate the high density of the relatively straight primary screw dislocations with $0.5a[1\,1\,1]$ Burgers vectors although the coplanar array of secondary dislocations with Burgers vector $0.5a[1\,\bar{1}\,1]$ are also seen. The foil elsewhere in many areas contained almost equal amounts of primary and secondary screw dislocations as shown in Figs 3a, b and c. The density of forest screw dislocations of Burgers vector $0.5a[\bar{1}\,1\,1]$ is very small but can be seen more clearly in Fig. 3c ($\boldsymbol{g} = \bar{1}\,1\,0$). It was, in general, found in this alloy exhibiting coarse slip that the dislocation arrangements were non-uniform within a single foil. Further, as already pointed out by Foxall and Statham [24], the inhomogeneity of dislocation substructure could be a result of distribution of strain within a slip band. Therefore, the different characteristic features of dislocation substructures observed are presented along with a possible cause either in terms of the effect of the substitutional alloying or in terms of interstitial solid solution with hydrogen.

The dislocations are not very straight but cusped and uniformly distributed with the Burgers vectors of alternating sign. In addition, several edge dipole segments (Fig. 3a) and loops (Fig. 3c) are also seen. Among other important features are the expanding dislocation configurations (Fig. 3b), twist walls consisting of cross grid of screw dislocations (Fig. 3a), and formation of cell structure parallel to $1\,1\,1$ and $1\,\bar{1}\,1$ directions (right-hand top of Fig. 3c). The dislocation density is fairly high, of the order of 10^{10} to 10^{11} cm^{-2} although exact estimates have not been made. A comparison of these observations with those of other authors in pure niobium, niobium–molybdenum and niobium–rhenium alloys [23–25] indicates that the high lattice frictional stress on both the edge and the screw dislocations as a result of alloying with vanadium is responsible for the relatively long, cusped dislocations with edge dipole segments. However, it is clear that the cell structure resolved in Fig. 3c has not been observed in either pure niobium or in alloys of niobium [23] at comparable strains, alloying content and temperature of deformation. We associate this effect with the high mobility of dislocations in local regions of enhanced hydrogen concentration due to secondary slip, also activated by hydrogen prematurely. On the other hand, twist wall boundaries such as those shown in Fig. 3a observed in pure niobium when deformed at much lower temperature, namely 77 K (see Figs 10 and 14 of [25]) are characteristic features associated with anomalous slip. The present observations do not support this association due to the absence of anomalous slip in the niobium–vanadium alloy.

Another typical substructure of the $(\bar{1}\,0\,1)$ cut foil is shown in Figs 4a and b. These illustrate the cusped and curved long screw dislocations which are more tangled in the thicker areas of the foil with very large density of loop debris and of loops of smaller size. These features are associated with smaller magnitude of frictional stress in pure niobium deformed at 158 K (see Fig. 12c of [24] and Fig. 19a of [25]). The frictional stress in niobium with 8 to 10 at % vanadium alloy at 195 K is larger than that in pure niobium at 158 K although a higher magnitude of strain could be responsible for cross slip and tangled structure with extensive loop formation. This result will be illustrated further through *in situ* observations.

Another important observation in the $(\bar{1}\,0\,1)$ cut foil is a band within which dislocation substructure is very fine as shown in Figs 5a and b. The band, as seen in Fig. 5a, is parallel to one set of the screw dislocations with Burgers vector $0.5a[1\,1\,1]$. The higher magnification picture of the band shown above in Fig. 5a illustrates the fine structure of dislocations within the band. This foil has been examined under several other two-beam conditions. Fig. 5b illustrates the fine

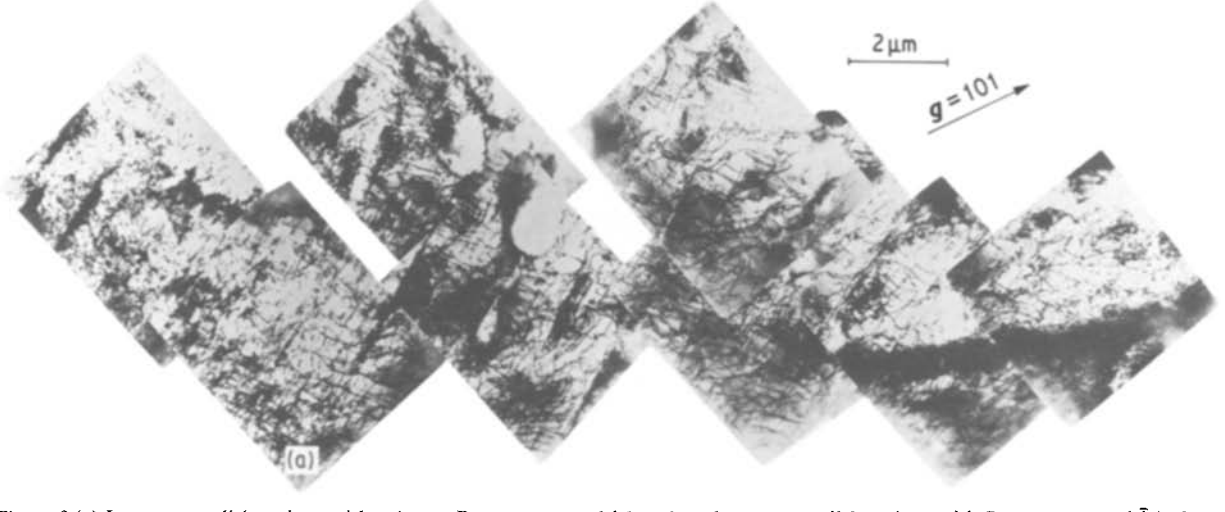

Figure 3 (a) Long screw dislocations with primary Burgers vector $1\,1\,1$ and coplanar screw dislocations with Burgers vector $1\,\bar{1}\,1$ observed in a foil cut parallel to $(\bar{1}\,0\,1)$ plane in specimen C_2. Other important features include formation of twist walls of screw dislocations and dislocation cell structure in the $1\,1\,1$ directions, $\varepsilon = 0.048$, $T = 195$ K, $\boldsymbol{b} = \bar{2}\,\bar{3}\,2$ and $\boldsymbol{g} = 1\,0\,1$. (b) Long screw dislocations with Burgers vector $\bar{1}\,1\,1$ and $1\,1\,1$ and cell structure observed in the foil cut parallel to $(\bar{1}\,0\,1)$ plane in crystal C_2, $\varepsilon = 0.048$, $T = 195$ K and $\boldsymbol{b} = \bar{1}\,\bar{3}\,3$. (c) Long screw dislocations with Burgers vector $\bar{1}\,1\,1$ and $1\,\bar{1}\,1$ and cell structure observed in the foil cut parallel to $(\bar{1}\,0\,1)$ plane in crystal C_2, $\varepsilon = 0.048$, $T = 195$ K and $\boldsymbol{b} = \bar{5}\,\bar{5}\,3$.

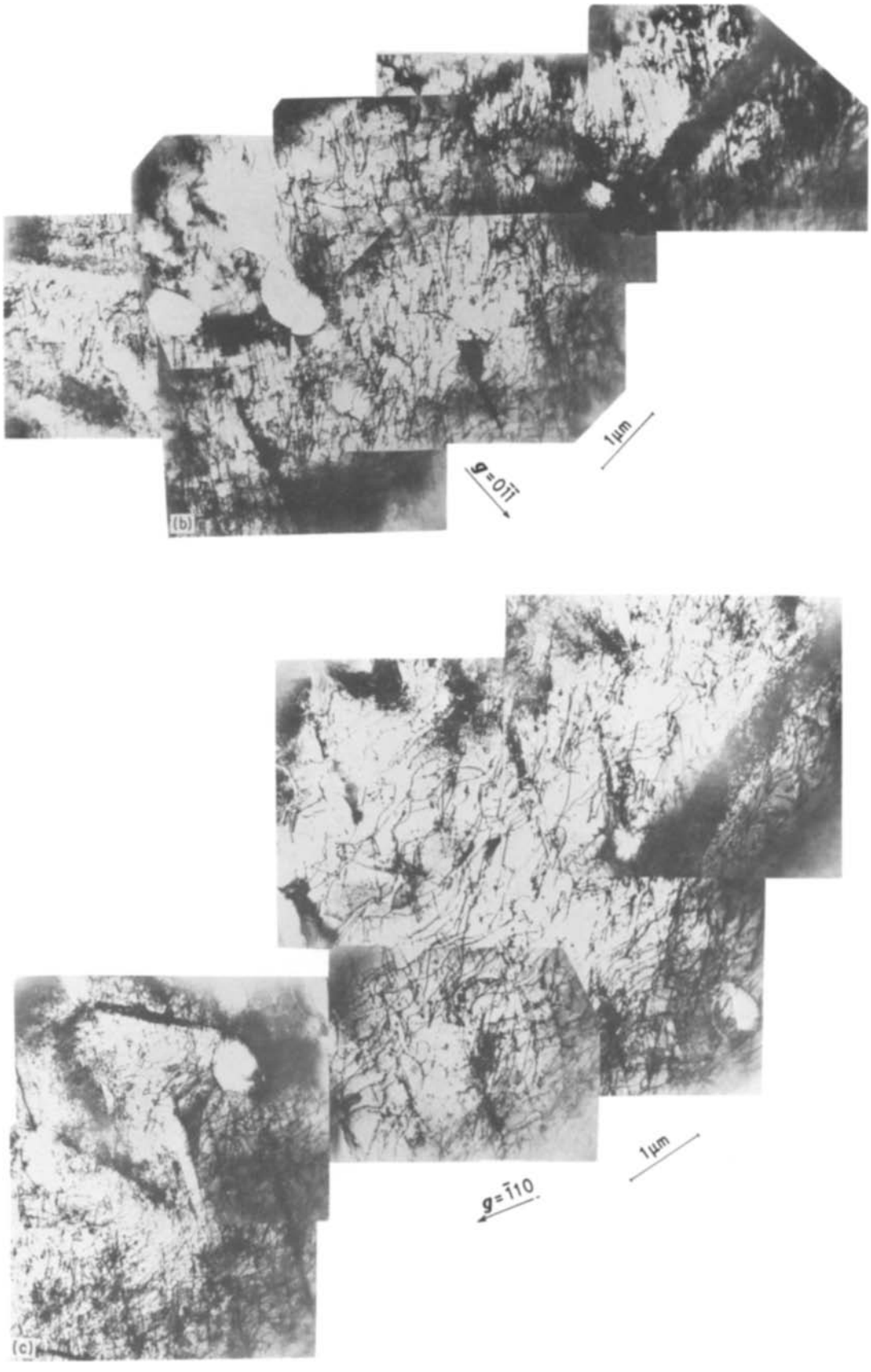

Figure 3 Continued.

dislocation substructure present in the area across the band. The substructure is different on either side of the band and so is the orientation of the foil, as determined from the shift in the diffraction pattern. The authors believe further observations are needed to confirm that these bands are similar to those observed by Garratt-Reed and Taylor [26] in pure niobium at 77 K which have been associated with anomalous slip. The presence of cross grid of screw dislocations and bands in the [1 1 1] directions in the niobium-rich niobium vanadium alloy at 195 K in the absence of anomalous slip indicates that the mechanism of anomalous slip

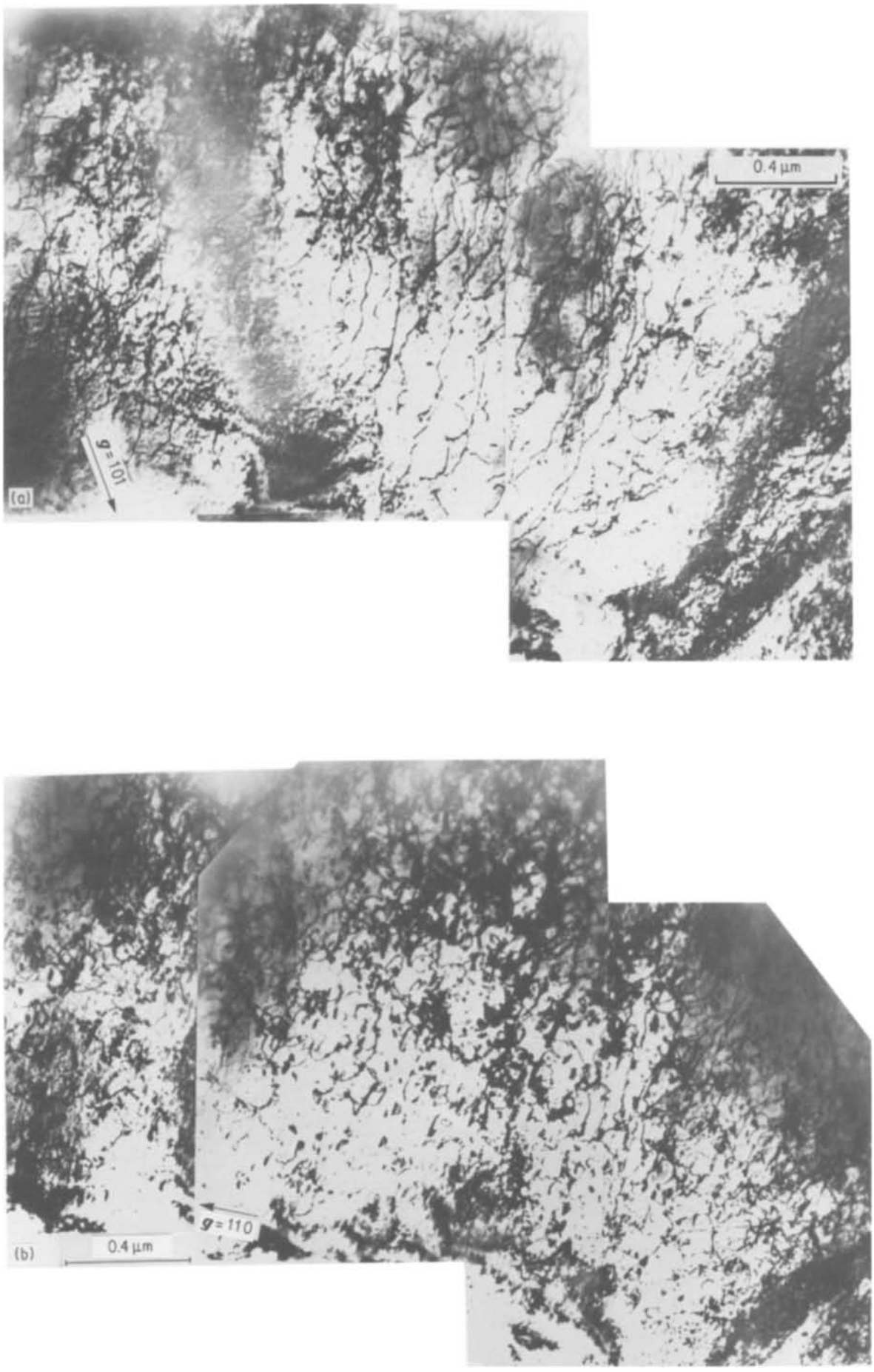

Figure 4 (a) Dislocation substructure consisting of long but not very straight primary screw dislocations with Burgers vector 1 1 1 forming tangles with dislocations of Burgers vector 1 $\bar{1}$ 1 in a foil cut parallel to a ($\bar{1}$ 0 1) plane in crystal C_2, $\varepsilon = 0.048$, $T = 195$ K and $\boldsymbol{b} = \bar{1}\,0\,1$. (b) Dislocation substructure consisting of primary screw dislocations with Burgers vector 1 1 1 interacting with secondary dislocations of Burgers vector 1 1 $\bar{1}$ leading to loop debris in the 1 1 2 directions observed in a foil cut parallel to ($\bar{1}$ 0 1) in crystal C_2, $\varepsilon = 0.048$, $T = 195$ K, and $\boldsymbol{b} = \bar{1}\,1\,1$.

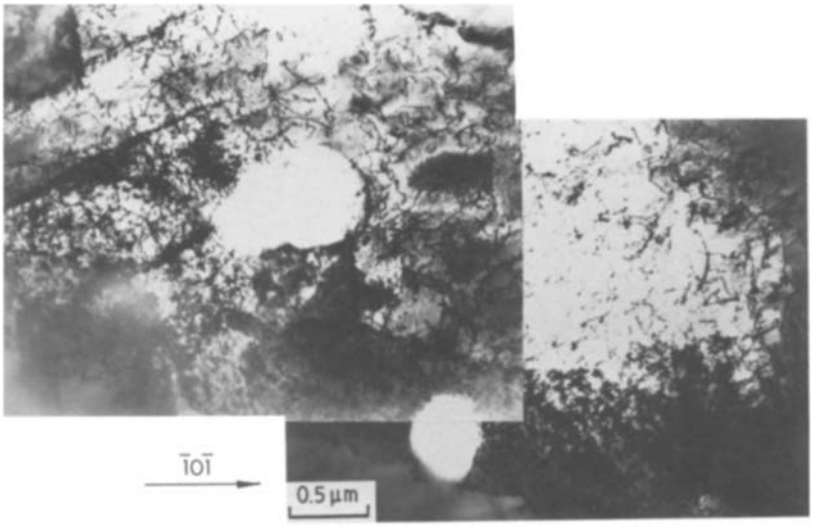

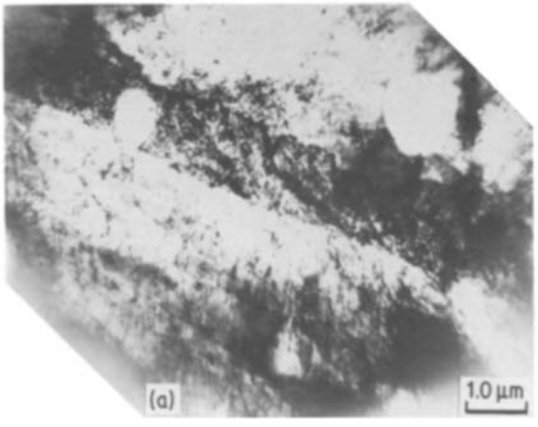

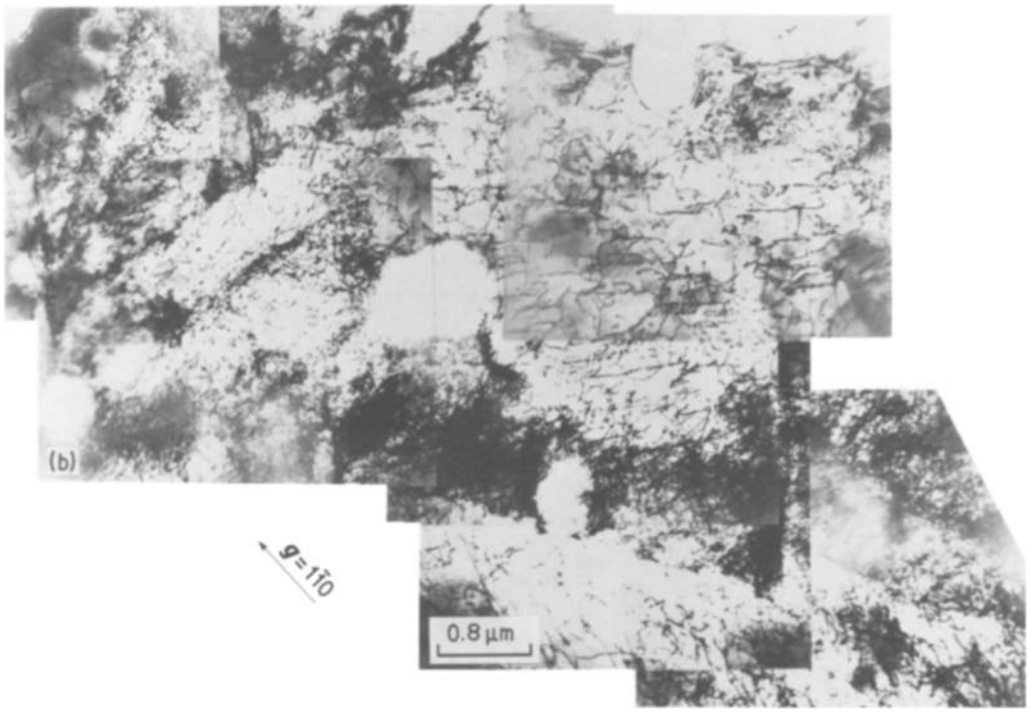

Figure 5 (a) Banded dislocation substructure in the 1 1 1 direction containing dislocation arrangement in a foil cut parallel to $(\bar{1}\,0\,1)$ plane in crystal C_2, $\varepsilon = 0.048$, $T = 195$ K and $\boldsymbol{b} = \bar{1}\,0\,1$. The low magnification picture below shows screw dislocations of Burgers vector 1 1 1 parallel to the band and screw dislocations of Burgers vector $1\,\bar{1}\,1$ inclined to the band. (b) Banded dislocation substructure containing dislocations with Burgers vector $\bar{1}\,1\,1$ and $1\,\bar{1}\,1$ in the foil cut parallel to the $(\bar{1}\,0\,1)$ plane in crystal C_2, $\varepsilon = 0.048$, $T = 195$ K and $\boldsymbol{b} = \bar{4}\,4\,3$.

described earlier [25] should be re-examined with additional experimental studies.

3.1.2. Foils cut parallel to (0 1 1) sections

The dislocation substructure in the foils cut parallel to the secondary slip plane (see Fig. 1) typically consists of cross grid of screw dislocations with Burgers vector $0.5a[1\,\bar{1}\,1]$ and $0.5a[\bar{1}\,\bar{1}\,1]$ as shown in Fig. 6a. On the other hand, loop debris and forest dislocations with Burgers vector $0.5a[1\,1\,1]$ were also observed in smaller density in addition to the straight screw dislocations of Burgers vector $0.5a[\bar{1}\,\bar{1}\,1]$. A comparison of dislocation substructures shown in Fig. 3 and in Fig. 6 suggests that the relatively straight dislocations in the (0 1 1) section are the result of a smaller percentage of strain that can be accounted on the secondary

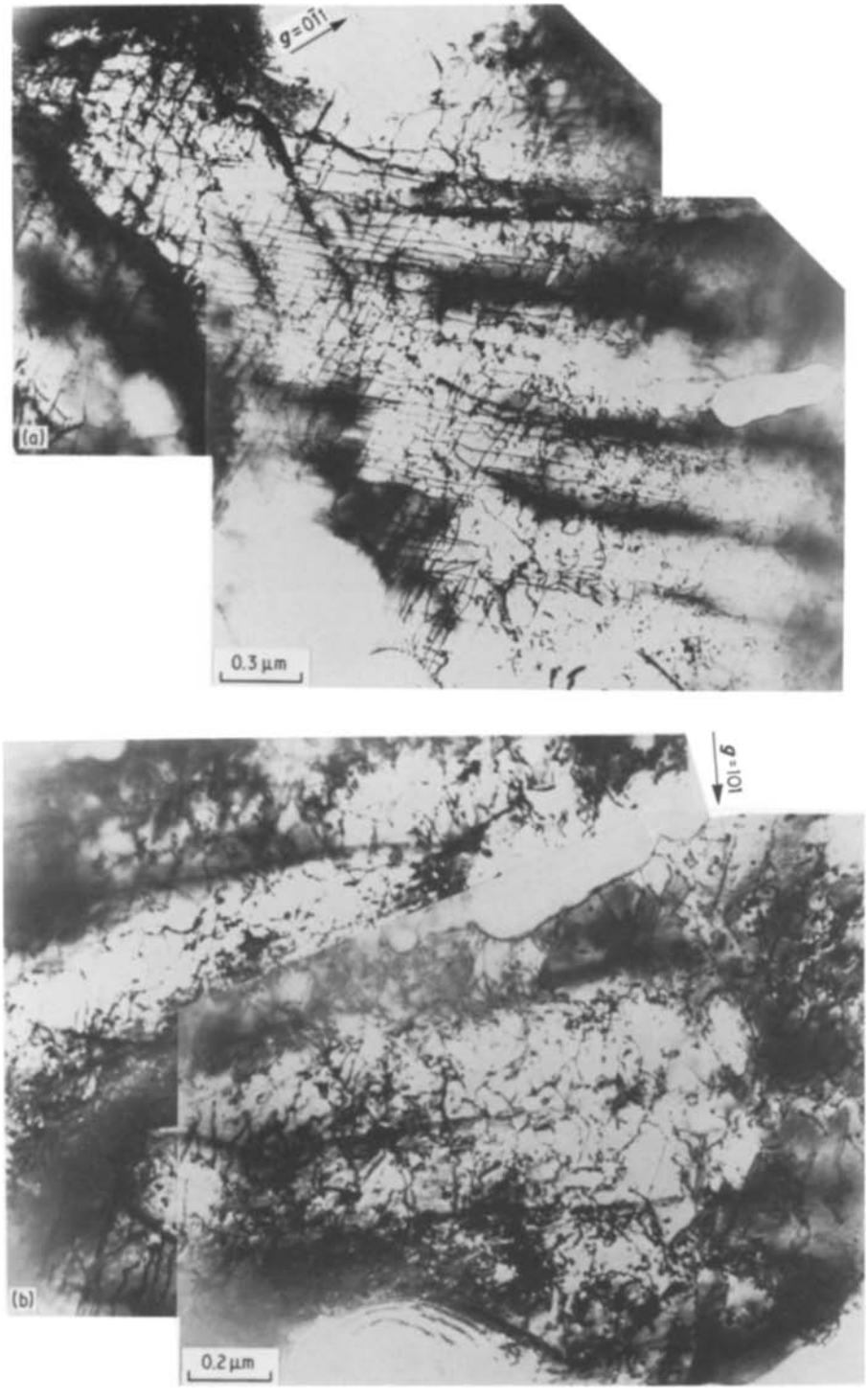

Figure 6 (a) Dislocation substructure consisting of twist wall boundary made up of straight cross grid of screw dislocations with Burgers vectors $1\bar{1}1$ and $\bar{1}\bar{1}1$ observed in a foil cut parallel to (0 1 1) plane in crystal C_2, $\varepsilon = 0.048$, $T = 195\,K$ and $\boldsymbol{b} = \bar{1}22$. (b) Dislocation substructure consisting of tangled dislocations with Burgers vector 1 1 1 and long dislocations with Burgers vector $\bar{1}\bar{1}1$ observed in the foil cut parallel to (0 1 1) plane in crystal C_2, $\varepsilon = 0.048$, $T = 195\,K$ and $\boldsymbol{b} = \bar{2}21$.

slip system compared to a larger percentage on the primary slip system. In other words, the straight screw dislocations in the array cross slip at higher stress levels giving rise to cusps, dipoles and loops, similar to those observed on the primary slip system.

3.2. Dislocation substructure in crystal 15_2

The initial orientation of the tensile axis of the crystal 15_2 which is not charged with hydrogen is also shown in Fig. 1 along with the poles of the primary $(\bar{1}\,0\,1)$ and the secondary (1 0 1) slip planes. Of these, only foils cut parallel to the $(\bar{1}\,0\,1)$ primary slip plane have been examined. The dislocation substructure shown in Figs 7a and b again consists of long primary screw dislocations of Burgers vector $0.5a[1\,1\,1]$ which are more curved and less straight. In addition, a cross grid of straight screw dislocations of Burgers vector $0.5a[1\,1\,1]$ and $0.5a[1\,\bar{1}\,1]$ and loop debris are also observed. These features, as previously illustrated, are also common to the dislocation substructure observed in crystal C_2 with hydrogen. However, the cell structure observed distinctly in crystal C_2 in the presence of hydrogen has not been observed in crystal 15_2.

The above observations of dislocation substructure in single crystals, although not very extensive but yet representative, illustrate that the presence of hydrogen introduces cell structure at early stages of deformation as a result of localized increase in dislocation density. On the other hand, the effect of vanadium as a substitutional alloying element is to increase the frictional stress on both edge and screw dislocations moderately at 195 K.

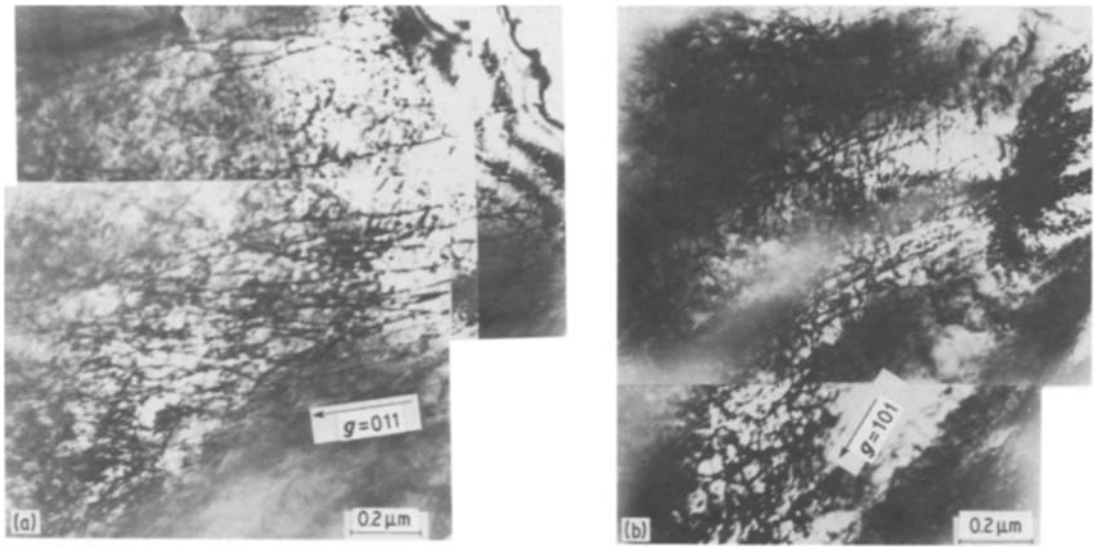

Figure 7 (a) Long parallel dislocation of Burgers vector 1 1 1 observed in a foil cut parallel to the primary slip plane ($\bar{1}$ 0 1) in crystal 15_2 of niobium–10 at % vanadium alloy. (b) Dislocation substructure consisting of cross grid of screw dislocations of Burgers vector 1 1 1 and 1 $\bar{1}$ 1 observed in a foil cut parallel to ($\bar{1}$ 0 1) plane in crystal 15_2 of niobium–10 at % vanadium alloy.

3.3. Dislocation substructure in polycrystalline specimens

3.3.1. Dislocation substructure in specimens deformed in tension

Fig. 8a shows the high density of long curved and tangled dislocations with loop debris observed in a specimen containing no hydrogen and deformed up to necking at 195 K. It can also be concluded from the alternating contrast that the dislocations are of opposite sign. On the other hand, Fig. 8b illustrates the rearrangement of dislocations into well-defined cell structure observed in the presence of 200 p.p.m. wt % hydrogen in a specimen deformed up to necking at 195 K. The less dense, relatively dislocation-free foil area outside the cell walls can also be identified. The dislocation substructure in the alloy deformed lightly at 195 K is presented in Figs 9a and b. Whereas the substructure in a specimen with 200 p.p.m. wt % hydrogen (Fig. 9a) consists of tangled dislocations and curved segments with high density of loop debris, the dislocation substructure in a specimen with 400 p.p.m. wt % hydrogen (Fig. 9b) consists of less tangled but curved and cusped dislocations, loop debris and patches of areas with high dislocation activity, consisting of small loops difficult to resolve. Further, the substructure observed in specimens with 200 p.p.m. wt % hydrogen and deformed lightly at 78 K has been found to consist of the same general features mentioned previously, namely long curved and cusped dislocations with a large amount of loop debris and tangled structure. On the other hand, the dislocation substructure in specimens deformed at room temperature showed very much tangled dislocations with the dislocation free link length being the smallest.

At this juncture, it is useful to point out that this alloy exhibited high ductility in the presence of hydrogen both at 77 and 295 K. On the other hand, the ductility is reduced only moderately at 195 K in the presence of hydrogen [19]. Thus, the reduction in ductility of the alloy is associated with the formation of cell structure in the presence of hydrogen at 195 K, both in single crystal and polycrystalline specimens. The cell walls are low-angle boundaries wherein hydrogen atoms accumulate due to local concentration

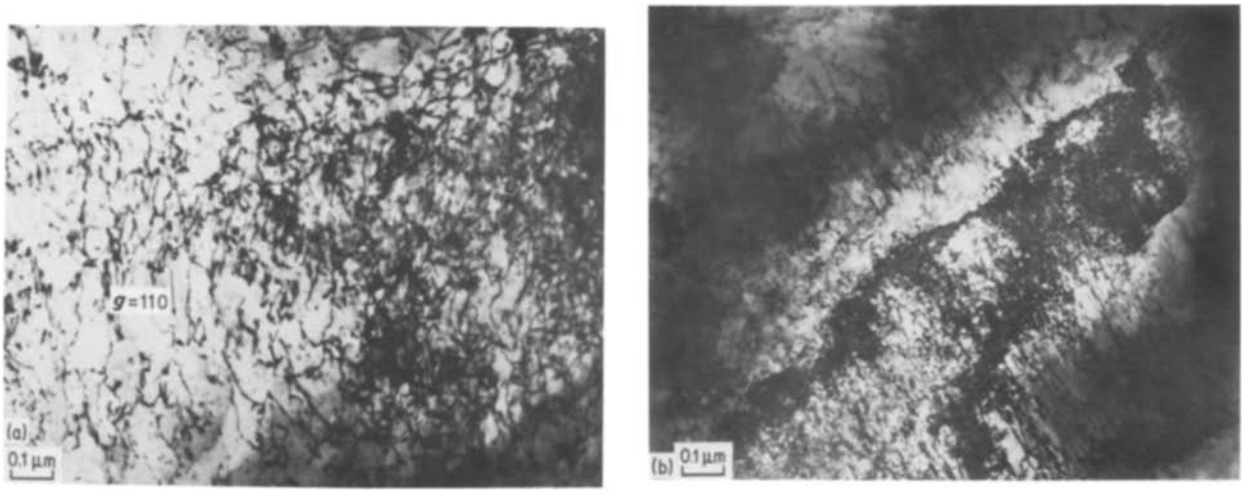

Figure 8 (a) Dislocation substructure observed in niobium–10 at % vanadium alloy tensile deformed up to necking at 195 K, $\boldsymbol{b}$ = $\bar{1}$ 1 3. (b) Dislocation substructure observed in niobium–10 at % vanadium alloy with 200 p.p.m. wt % hydrogen tensile deformed up to necking at 195 K, $\boldsymbol{b}$ = 0 0 1 and multiple $\boldsymbol{g}$ vectors are operating.

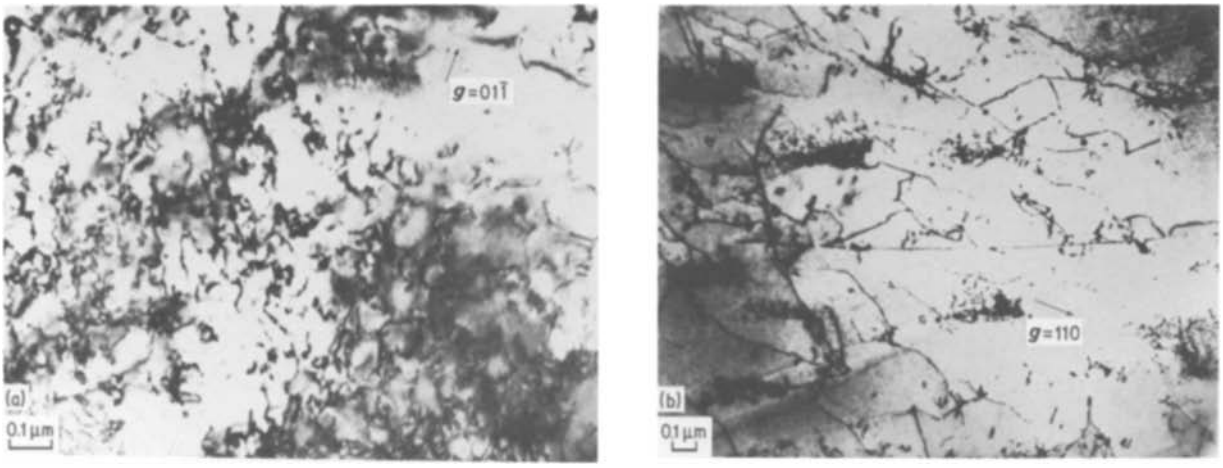

Figure 9 (a) Dislocation substructure observed in niobium–10 at % vanadium alloy with 200 p.p.m. wt % hydrogen tensile deformed lightly at 195 K, $\boldsymbol{b}$ = 1 1 1. (b) Dislocation substructure observed in niobium–10 at % vanadium alloy with 400 p.p.m. wt % hydrogen tensile deformed lightly at 195 K, $\boldsymbol{b}$ = 0 0 1.

of stress field. There is considerable evidence to show that cell walls become nucleation centres for cracks [9] and consequently the presence of high hydrogen concentration should help the nucleation and propagation of cracks. The mobility of hydrogen atoms as well as that of the dislocations is considerably reduced at 77 K so that the conditions for both the formation of cell structure and accumulation of hydrogen atoms are unfavourable. On the other hand, hydrogen atoms are mobile at 195 K so that accumulation along cell walls is favourable. The large ductility in the alloy at 295 K is expected due to high diffusivity of hydrogen so that a sufficiently large concentration cannot be maintained. In addition, the stress concentration can be reduced readily by extensive local plastic deformation that takes place due to lower yield stress at room temperature.

3.3.2. Dislocation substructure in specimens deformed in compression

The dislocation substructure shown in Figs 10a and b illustrate the presence of cross grid of straight long

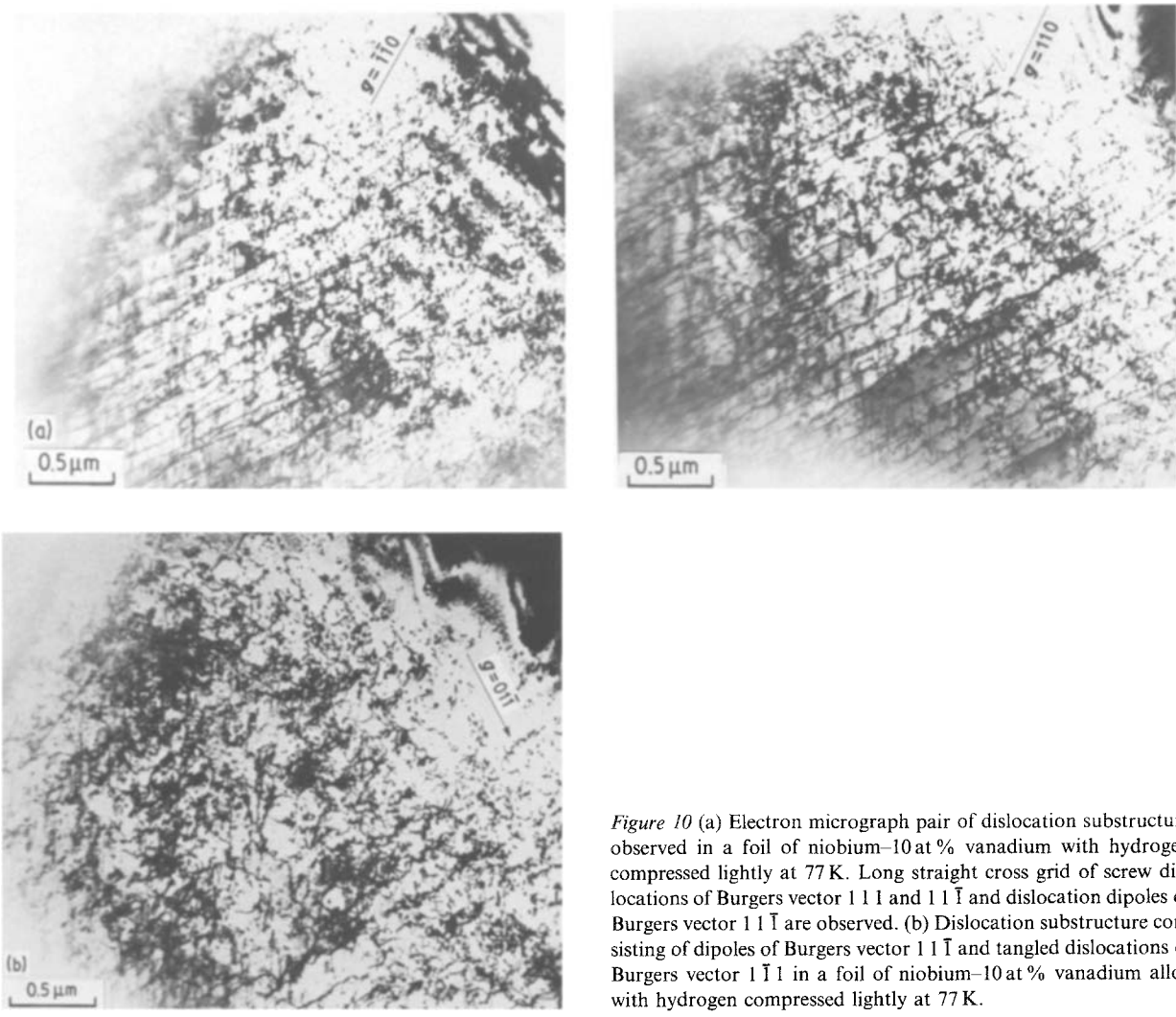

Figure 10 (a) Electron micrograph pair of dislocation substructure observed in a foil of niobium–10 at % vanadium with hydrogen compressed lightly at 77 K. Long straight cross grid of screw dislocations of Burgers vector 1 1 1 and 1 1 $\bar{1}$ and dislocation dipoles of Burgers vector 1 1 $\bar{1}$ are observed. (b) Dislocation substructure consisting of dipoles of Burgers vector 1 1 $\bar{1}$ and tangled dislocations of Burgers vector 1 $\bar{1}$ 1 in a foil of niobium–10 at % vanadium alloy with hydrogen compressed lightly at 77 K.

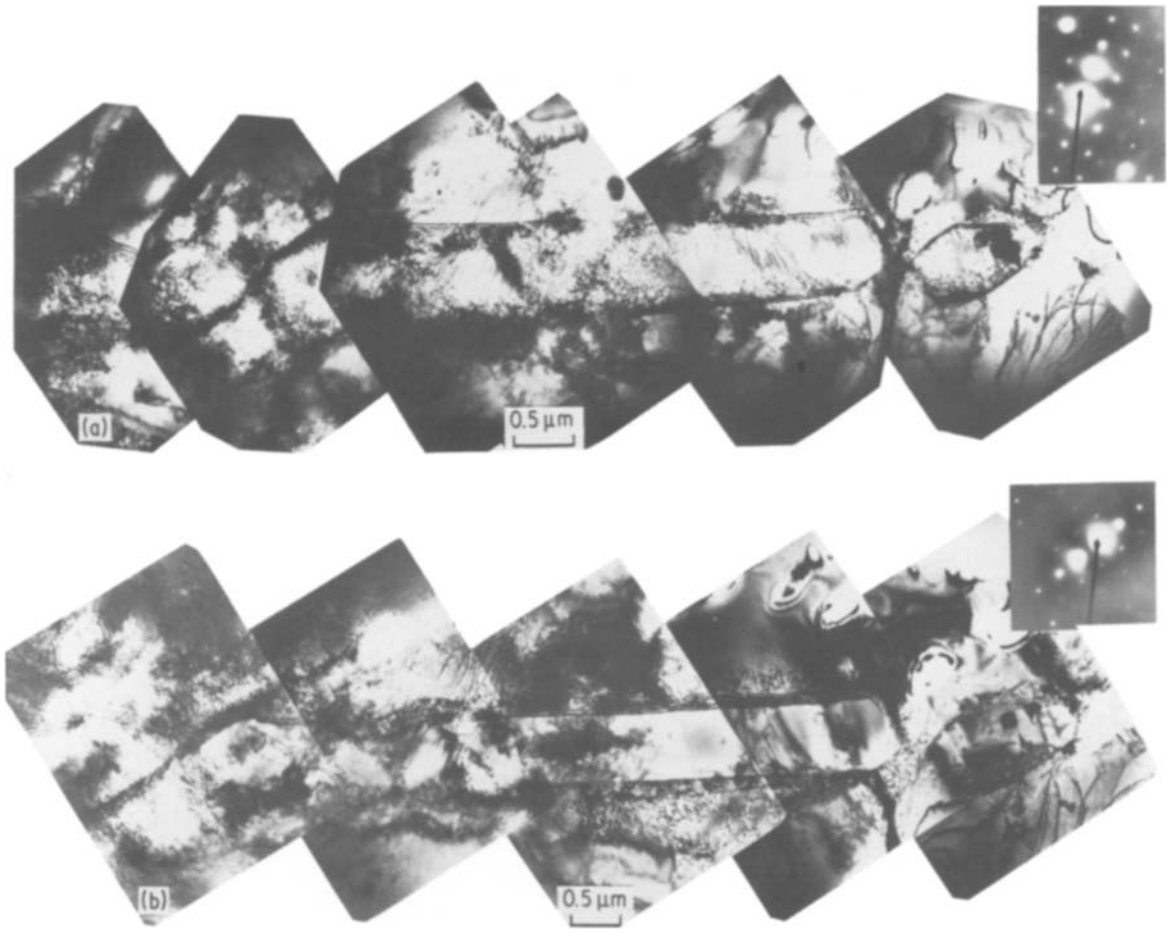

Figure 11 (a) Dislocation substructure inside a twinned region observed in a foil of niobium–10 at % vanadium alloy with hydrogen compressed lightly at 77 K. (b) Dislocation substructure in the matrix surrounding a twinned region observed in the foil of niobium–10 at % vanadium alloy with hydrogen compressed lightly at 77 K.

screw dislocations of Burgers vector $0.5a[1\,1\,1]$ and $0.5a[1\,1\,\bar{1}]$, frequently of alternating sign observed in a specimen containing 200 p.p.m. wt % hydrogen and deformed lightly at 77 K. In addition, dipoles of Burgers vector $0.5\,a[1\,1\,\bar{1}]$ can easily be identified from the alternating light and dark shades of contrast (Fig. 10a). Furthermore, the foil also contained large density of dislocation loop debris and tangled dislocations of Burgers vector $0.5a[1\,\bar{1}\,1]$ (Fig. 10b). A comparison of substructure shown in Fig. 10 with that in Fig. 6, both of which are observed for small strains illustrates that the straight long screw dislocations in the initial stages of deformation transform with increasing strain into a more curved and cusped dislocation and further into a well-defined cell structure in the presence of hydrogen as seen in Fig. 3.

The preparation of foils containing twins has been much easier from compressed polycrystalline specimens since twinning is profuse in compression at 77 K while it is absent in tension. Further, the identification of the twin and the matrix regions is carried out by tilting the foil such that when the matrix belongs to the $\bar{1}\,1\,1$ zone, the twin belonged to the $\bar{1}\,1\,5$ zone and vice versa and when the matrix belonged to the $\bar{1}\,1\,2$ zone, the twin also belonged to the same zone assuming that the twin habit plane is $(\bar{1}\,1\,2)$. The dislocation substructure associated with a twin is shown in Figs 11a and b. In particular, the twinned region appears to have grown in steps under the applied compressive stress, as seen from several twinned segments in the form of lamallae. Alternately, the stress concentration associated with a terminating twin could give rise to the next segment [22]. Whereas a detailed analysis of the dislocation substructure associated with the twin (Fig. 11a) and with the matrix (Fig. 11b) will be published subsequently, it is seen that the dislocations did not cut through the interface at one end but in an adjacent area the straight dislocations in the matrix passed through the interface into the twin, thus producing a ledge step. The stress concentration where the dislocations did not pass through the interface is apparently relieved by the generation of dislocation substructure in the matrix. The twin–matrix interface is heavily dislocated due to deformation associated with each region suggesting that twins obstruct continuation of slip in the initial stages of deformation. However, with increasing deformation, slip eventually propagates through the interface into the twin. By the same token, twins in this alloy cannot readily be the centres for nucleation of cracks since the matrix relieves the stress concentration by accommodation slip, i.e. generation of dislocations.

4. Discussion

The effect of 8 to 10 at % vanadium as a substitutional alloying element should be separated from the effect of interstitial hydrogen in understanding the development of dislocation substructure in this alloy. The

cross grid of straight screw dislocations and edge dipole configurations in the initial stages of deformation at 195 K clearly indicate the presence of high frictional stress to the movement of both screw and edge dislocations and to cross slip which should be attributed to the substitutional alloying effect. The more curved and cusped dislocations with loop debris observed at higher strains suggest that the stress field of the neighbouring dislocations in the array aids the applied stress in overcoming the frictional stress to cross slip in addition to slip that continues on the primary slip system.

On the other hand, formation of cell structure and regions of high dislocation density at 195 K should be attributed to the enhanced dislocation mobility in the presence of hydrogen with considerably high diffusivity. This result also supports the observation of the nucleation and propagation cracks along active slip planes in the presence of hydrogen at 195 K [21]. The effect of hydrogen on the dissociated core structure of screw dislocations is not directly revealed in these observations. Thus, while deformation twinning becomes more pronounced in the presence of hydrogen, there is scant evidence such as the formation of faulted configurations to suggest that it is the outcome of lowered stacking fault energy. On the other hand, the increased frictional stress on the screw and edge dislocations through the stress field interaction with the tetragonal distortion associated with the interstitial gives rise to a more planar array of straight dislocations at 77 K where the mobility of hydrogen is also low. The stress concentration associated with the planar array in the early stages of deformation aids the formation of stable twins by overcoming the activation energy required for twinning [20, 21]. There is growing evidence to suggest that a stress concentration gives rise to deformation twins in other similar situations [26, 27]. Thus, any prior deformation at a higher temperature to introduce a more uniform tangled dislocation substructure eliminates the possibility of twinning during subsequent deformation at a lower temperature, a result which is observed experimentally [28]. The substructural features associated with twins in this alloy suggest that crack nucleation cannot be linked with the presence of twins in this alloy.

It is now useful to examine the effect of neighbouring dislocations on the stress required for screw dislocations to cross slip. Earlier estimates of the behaviour of screw dislocations to cross slip has neglected this effect [25]. The configuration studied is shown in Fig. 12 where two pairs of parallel screw dislocations of Burgers vector $0.5a[1\,1\,1]$ situated on two parallel primary $(\bar{1}\,0\,1)$ slip planes tend to cross slip on to either the $(\bar{2}\,1\,1)$ or the $(\bar{1}\,1\,0)$ plane. The starting configuration is determined by the initial distance between the innermost screw dislocations, X_i between the two parallel dislocations of like sign, X_d between the two parallel $(\bar{1}\,0\,1)$ planes, D and the frictional stress, τ_f to movement of dislocations which is assumed to be the same on the primary and cross slip planes. The equilibrium configuration is determined by minimization of the total energy of the configuration with respect to the positions of the dislocations in the presence of both the applied stress and the frictional stress. Since the frictional energy associated with the movement of dislocations is always positive and the conditions of force equilibrium do not necessarily correspond to the minimum of the total energy of the configuration [29], it has become imperative to use the energy minimization. In addition, the energy of the configuration is dependent on the path of dislocations and hence the equilibrium is determined by incrementing the applied stress, τ, by a very small value so that false minima are not obtained. The numerical calculations of the energy are performed using the parameters pertinent to this alloy, i.e. shear modulus = $\mu = 4.037 \times 10^{11}$ dyn cm^{-2} and Burgers vector, $\boldsymbol{b}$ = 0.285 nm. In particular, the total energy minimized is given by

$$E_t = E_s + E_i + E_w + E_f \qquad (1)$$

where E_s is the self energy term and E_i the interaction energy term associated with the dislocations, E_w the work done by the applied stress in moving the dislocations from their initial positions and E_f the frictional energy term spent in moving the dislocations. The self energy and the interaction energy terms associated with dislocations are determined from standard formulae applicable to parallel dislocations [29]. On the other hand, the work done by the applied stress is given by

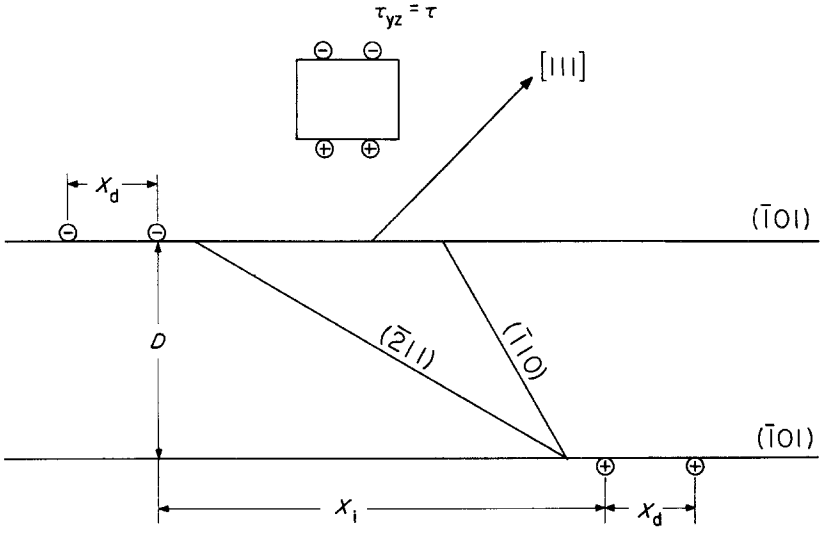

Figure 12 A schematic illustration of two pairs of screw dislocations on the primary $(\bar{1}\,0\,1)$ slip planes considered to cross slip on to $(\bar{2}\,1\,1)$ or $(\bar{1}\,1\,0)$ plane under the action of applied shear stress, τ and the mutual attractive and repulsive forces.

$$E_w = \sum_{j=1}^{4} \tau b_j (X_i - X_f) \quad (2)$$

where X_i and X_f are the initial and final projected distances of each dislocation on to the primary slip plane. In addition, E_f is given by

$$E_f = E_{f_0} + \sum_{j=1}^{4} \tau_f b_j |X_{j_0} - X_{j_1}| \quad (3)$$

where E_{f_0} is the value of the frictional energy and X_{j_0} the position at the previous value of applied stress while X_{j_1} is the new position of the dislocation after incrementing the applied stress. It should be noted that the values of the positions in Equation 3 are the actual and not the projected distances when the dislocations move on the cross slip plane and only a positive value of $X_{j_0} - X_{j_1}$ should be considered. Whereas, the details of minimization program are available elsewhere [30], it has been found that the accuracy of minimization as well as the magnitude of the increment of applied stress are important. There is only one $(\bar{2}\,1\,1)$ or $(\bar{1}\,1\,0)$ slip plane along which the symmetrical dislocation configuration can cross slip before annihilation of opposite sign dislocations takes place.

The results of the numerical analysis are illustrated in Figs 13a and b. Specifically, the applied stress required to move the nearest screw dislocations on the $(\bar{1}\,0\,1)$ primary slip plane is shown as a function of τ_f for $D = 600\boldsymbol{b}$ in Fig. 13 by joining the various points with continuous lines for three values of initial positions of dislocations, $X_i = X_d$. On the other hand, the magnitude of applied stress for cross slip on to either the $(\bar{2}\,1\,1)$ or $(\bar{1}\,1\,0)$ is indicated in the diagram without being joined together. Thus for example when $\tau_f = 1.0 \times 10^8$ dyn cm^{-2}, cross slip on to both the $(\bar{2}\,1\,1)$

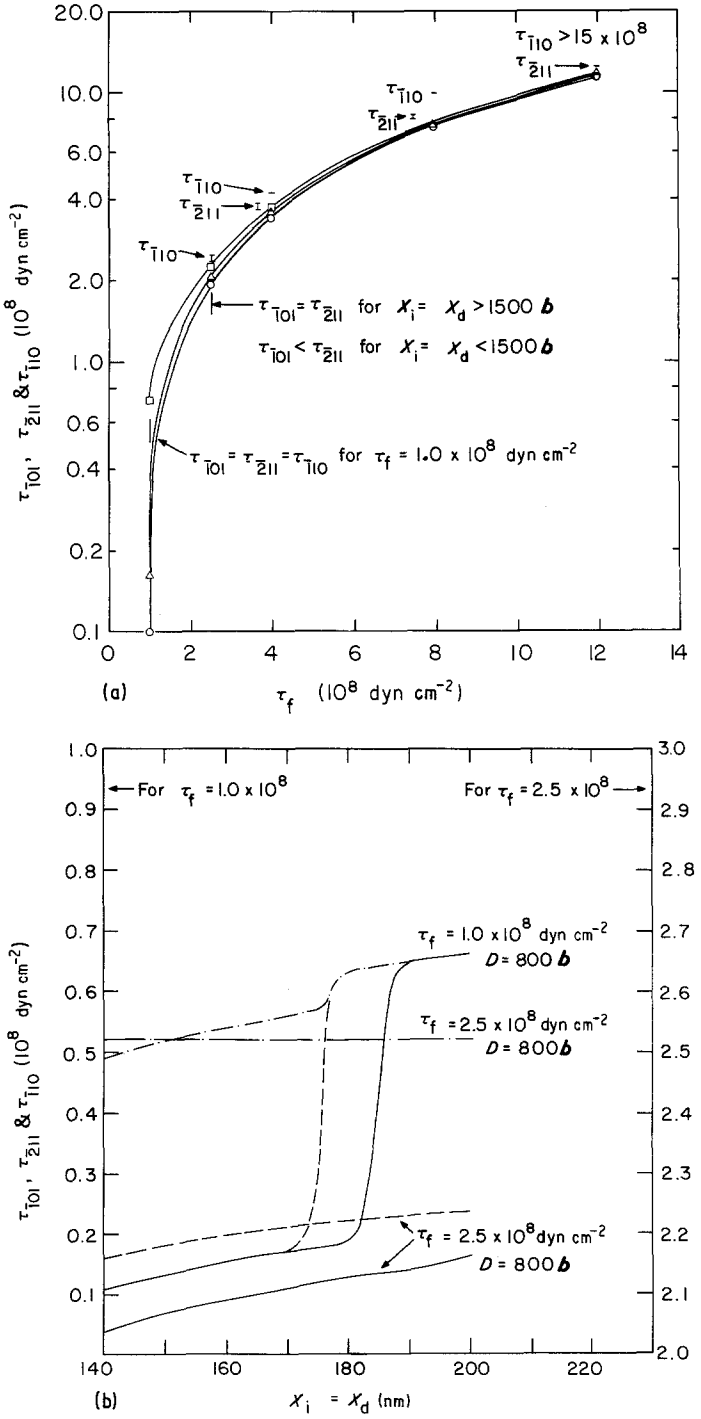

Figure 13 (a) The magnitude of applied shear stress at which the two nearest screw dislocations of opposite sign move on (a) the primary $(\bar{1}\,0\,1)$ slip plane ($\tau_{\bar{1}01}$), (b) the $(\bar{2}\,1\,1)$ cross slip plane ($\tau_{\bar{2}11}$) and (c) the $(\bar{1}\,1\,0)$ cross slip plane ($\tau_{\bar{1}10}$) shown as a function of τ_f for $D = 600\boldsymbol{b}$ and different values of $X_i = X_d$: (○) $1100\boldsymbol{b}$, (△) $1500\boldsymbol{b}$, (□) $2500\boldsymbol{b}$. (b) The magnitude of applied shear stress at which the two nearest screw dislocations of opposite sign move on (——) the primary $(\bar{1}\,0\,1)$ slip plane ($\tau_{\bar{1}01}$), (– – –) the $(\bar{2}\,1\,1)$ cross slip plane ($\tau_{\bar{2}11}$) and (–·–·–) the $(\bar{1}\,1\,0)$ cross slip plane ($\tau_{\bar{1}10}$) shown as a function of $X_i = X_d$ for two values of τ_f and $D = 800\boldsymbol{b}$.

and $(\bar{1}\,1\,0)$ takes place readily after the dislocations start to move on the primary slip plane, although $\tau_{\bar{1}01}$ itself increases with increasing $X_i = X_d$, showing the effect of adjacent dislocations. On the other hand, when τ_f is increased to 2.5×10^8 dyn cm^{-2}, $\tau_{\bar{1}10}$ for all three values of $X_i = X_d$ is much larger implying cross slip is not favourable at $\tau_{\bar{1}01}$. However, for the same τ_f cross slip on to $(\bar{2}\,1\,1)$ is favourable at τ_{101} only for $X_i = X_d > 1500\boldsymbol{b}$. An important point to note is that while dislocation movement on $(\bar{1}\,0\,1)$ and as a result dipole formation is favourable for $X_i = X_d < 1500\boldsymbol{b}$, cross slip becomes possible on to either the $(\bar{2}\,1\,1)$ or $(\bar{1}\,1\,0)$ planes when the applied stress is raised to the required magnitude. These results are equally applicable at other higher values of τ_f although the stress at which cross slip takes place remains much higher than $\tau_{\bar{1}01}$, as shown in Fig. 13. This implies that the change from the substructure containing straight screw dislocations to that containing edge segments in the curved and cusped dislocations, and dislocation loops takes place at a higher value of applied stress or plastic strain. If the initial positions of like dislocations in each $(\bar{1}\,0\,1)$ plane are further apart, the lattice frictional stress keeps them apart during subsequent dislocation motion so that $\tau_{\bar{1}01} = \tau_{\bar{2}11}$.

The results for $D = 800\boldsymbol{b}$ and two values of τ_f are shown in Fig. 13b wherein it should be noted that two different scales are used to represent τ at two values of τ_f. In addition, the importance of the initial separation between the two like dislocations is illustrated in Fig. 13b. In particular, if $X_i = X_d > 1900\boldsymbol{b}$, $\tau_{\bar{1}01}$ is large enough so that cross slip takes place on both $(\bar{2}\,1\,1)$ and $(\bar{1}\,1\,0)$ planes for $\tau_f = 1.0 \times 10^8$ dyn cm^{-2}. The difference in magnitude of $\tau_{\bar{1}01}$, $\tau_{\bar{2}11}$ and $\tau_{\bar{1}10}$ is also found to decrease with increasing $X_i = X_d$ for $\tau_f = 2.5 \times 10^8$ dyn cm^{-2}. It has also been verified in all these calculations that cross slip is accompanied by annihilation of opposite sign dislocations. In a more general situation, cross slip can take place on two parallel cross slip planes and as a result the opposite sign dislocations do not annihilate.

5. Conclusions

The dislocation substructures, developed in the niobium–8 to 10 at % vanadium alloy single crystal and polycrystalline specimens containing either no hydrogen or different percentages of hydrogen and deformed under different conditions have been observed. The observations enable the following conclusions to be made.

1. The straight long screw dislocations and dislocation dipoles observed in the initial stages of deformation are the outcome of increased frictional stress on both edge and screw dislocations due to alloying with substitutional vanadium. The more curved and cusped dislocations with edge dipole segments and loop debris observed at larger strains is a result of cross slip at higher stress levels.

2. The formation of cell structure in the early stages of deformation at 195 K is associated with the high diffusivity of interstitial hydrogen atoms giving rise to locally a higher dislocation density by operation of secondary slip.

3. The accumulation of hydrogen atoms along the cell walls due to the stress field interaction gives rise to easier crack nucleation and propagation along the slip planes.

4. The presence of stress concentration due to long straight screw dislocations is responsible for the reduction in activation energy for twinning so that stable twins grow in the absence of crack formation at 77 K.

5. The dislocation substructure associated with the deformation twins indicates that crack nucleation in the presence of hydrogen cannot be linked to twinning in this alloy.

Acknowledgements

The authors take this opportunity to thank Mr Lester K. Reed for the help in mechanical testing of the specimens, Mr Harlan H. Baker in preparing the specimens metallographically and Mr Charles V. Owen for the help in the use of the laboratory facilities. The help of the scientific and technical staff of the Materials Preparation Center, in particular Mr Frederick A. Schmidt, Mr John T. Wheelock, Mr Lanny P. Lincoln and Mr Marv E. Thompson in preparing the alloys is very much appreciated. The work was performed for the United States Department of Energy, Office of Basic Energy Sciences, Division of Materials Sciences, under contract number: W-7405-Eng-82. The manuscript was presented at the symposium on Refractory Metals at the AIME Fall Meeting, 1984, Detroit, Michigan, U.S.A.

References

1. T. TABATA and H. K. BIRNBAUM, *Scripta Metall.* **17** (1983) 947.
2. *Idem, ibid.* **18** (1984) 231.
3. C. D. BEACHEM, *Met. Trans.* **3** (1972) 437.
4. B. A. WILCOX and G. C. SMITH, *Acta Metall.* **12** (1964) 317.
5. I. R. KRAMER and J. P. HIRTH, *Scripta Metall.* **18** (1984) 539.
6. I. M. ROBERTSON and H. K. BIRNBAUM, *ibid.* **18** (1984) 269.
7. W. A. McINTEER, W. A. THOMPSON and I. M. BERNSTEIN, *Acta Metall.* **28** (1980) 887.
8. K. JAGANNADHAM and FRANCIS C. LAABS, *J. Mater. Sci.* **22** (1987) 818.
9. H. G. F. WILSDORF, *Mat. Sci. Engng.* **59** (1983) 1.
10. J. P. HIRTH, *Met. Trans.* **11A** (1980) 861.
11. J. F. MILLER and D. C. WESTLAKE, *Trans. J. Inst. Metals* **21** (1980) 153.
12. G. WELSCH, R. GIBALA and T. E. MITCHELL, *Phys. Status Solidi* **30A** (1975) 117.
13. J. P. HIRTH and B. CARNAHAN, *Acta Metall.* **26** (1978) 1795.
14. P. B. HIRSCH, 5th International Conference on Crystallography, Oral communication, Cambridge (1960) p. 139.
15. L. P. KUBIN, in "Hardening of Metals", Vol. 3, edited by P. Feltham (Trans. Tech. SA, Aldermannsdorf, Switzerland, 1980) p. 67.
16. S. MAHAJAN, in "Mechanical Properties of B.C.C. Metals", edited by Meshii (The Metallurgical Society of AIME, Warrendale, Pennsylvania, 1982).
17. K. JAGANNADHAM, to be published.
18. C. V. OWEN, D.-S. CHEONG and T. E. SCOTT, *Met. Trans.* **15A** (1984) 147.
19. V. VITEK and J. W. CHRISTIAN, in "International Conference on Strength of Metals and Alloys", Vol. 1 (Institute of Metals, Cambridge, 1973) p. 534.

20. R. W. ARMSTRONG and P. J. WORTHINGTON, in "Metallurgical Effects at high strain rates", edited by R. W. Rhode, B. M. Butcher, J. R. Holland and C. H. Karnes (Plenum, New York, 1973).
21. K. JAGANNADHAM, submitted for publication.
22. S. MAHAJAN, *Met. Trans. A* **12** (1981) 379.
23. R. A. FOXALL and C. D. STATHAM, *Acta Metall.* **18** (1970) 1147.
24. G. TAYLOR and J. W. CHRISTIAN, *Phil. Mag.* **15** (1967) 893.
25. A. J. GARRATT-REED and G. TAYLOR, *ibid.* **39** (1979) 597.
26. C. HWANG and I. M. BERNSTEIN, *Scripta Metall.* **16** (1982) 85.
27. SHENG-TI FONG, M. J. MARCINKOWSKI and K. SADANANDA, *Acta Metall.* **21** (1973) 799.
28. N. A. BOUCHER and J. W. CHRISTIAN, *ibid.* **20** (1972) 581.
29. J. P. HIRTH and J. LOTHE, "Theory of Dislocations" (McGraw Hill, New York, 1968).
30. K. JAGANNADHAM and M. J. MARCINKOWSKI, "Unified Theory of Fracture" (Trans. Tech SA, Aldermannsdorf, Switzerland, 1983).

Received 13 November 1985
and accepted 30 June 1986